

QUALITATIVELY CHARACTERIZING NEURAL NETWORK OPTIMIZATION PROBLEMS

Ian J. Goodfellow* & Oriol Vinyals* & Andrew M. Saxe**

*Google Inc., Mountain View, CA

**Department of Electrical Engineering, Stanford University, Stanford, CA

{goodfellow, vinyals}@google.com, asaxe@stanford.edu

ABSTRACT

Training neural networks involves solving large-scale non-convex optimization problems. This task has long been believed to be extremely difficult, with fear of local minima and other obstacles motivating a variety of schemes to improve optimization, such as unsupervised pretraining. However, modern neural networks are able to achieve negligible training error on complex tasks, using only direct training with stochastic gradient descent. We introduce a simple analysis technique to look for evidence that such networks are overcoming local optima. We find that, in fact, on a straight path from initialization to solution, a variety of state of the art neural networks never encounter any significant obstacles.

1 INTRODUCTION

Neural networks are generally regarded as difficult to optimize. The objective functions we must optimize in order to train them are non-convex and there are not many theoretical guarantees about the performance of the most popular algorithms on these problems. Nevertheless, neural networks are commonly trained successfully and obtain state of the art results on many tasks.

In this paper, we present a variety of simple experiments designed to roughly characterize the objective functions involved in neural network training. These experiments are not intended to measure any specific quantitative property of the objective function, but rather to answer some simple qualitative questions. Do neural networks enter and escape a series of local minima? Do they move at varying speed as they approach and then pass a variety of saddle points?

Answering these questions definitively is difficult, but we present evidence strongly suggesting that the answer to all of these questions is no. We show that there exists a linear subspace in which neural network training could proceed by descending a single smooth slope with no barriers. Early symmetry breaking is the most conspicuous example of non-convexity.

One important question is what happens after SGD leaves this well-behaved linear subspace. The main text of this article is restricted to experiments that were peer-reviewed prior to ICLR 2014, but the appendix presents additional experiments added after the review process ended. These experiments show that in some cases SGD does encounter obstacles, such as a ravine that shapes its path, but we never found evidence that local minima or saddle points slowed the SGD trajectory. This suggests that less exotic problems such as poor conditioning and variance in the gradient estimate are the primary difficulties in training neural networks.

In all cases, we examine the total cost function (added up across all training examples). SGD of course only ever acts on unbiased stochastic approximations to this loss function. The structure of these stochastic approximations could be different from the global loss functions that we examine here, so it remains possible that neural networks are difficult to train due to exotic structures in individual terms of the total cost function, or due to the noise induced by sampling minibatches of these terms.

The results of our linear subspace experiments were qualitatively the same for all seven models we examined, which were drawn from a variety of categories, including fully-connected supervised feed-forward networks (Rumelhart et al., 1986) with a variety of activation functions, supervised

convolutional networks (LeCun et al., 2010), unsupervised models, recurrent models of sequences, and analytically tractable factored linear models. (The additional experiments in the appendix found some qualitatively unique behavior outside this linear subspace for two of our models, but the remainder have the same qualitative behavior as factored linear models)

Our models were all chosen because they performed well on competitive benchmark tasks. More research is needed to determine whether one should interpret our results as implying that SGD never encounters exotic obstacles when training neural networks, or as implying that SGD only works well when it does not encounter these structures.

2 LINEAR PATH EXPERIMENTS

Training a neural network consists of finding the optimal set of parameters θ . These are initialized to some set of small, random, initial parameters $\theta = \theta_i$. We then train using stochastic gradient descent (usually with extra features such as momentum) to minimize $J(\theta)$ until reaching convergence (usually some early stopping criterion). At the end of training, $\theta = \theta_f$.

The trajectory that SGD follows from θ_i to θ_f is complicated and high-dimensional. It is difficult to summarize such a trajectory meaningfully in a two-dimensional visualization. Simple learning curves showing the value of the objective function over time do not convey some fairly simple information. For example, when a learning curve bounces up and down repeatedly, we do not know whether the objective function is highly bumpy or whether SGD is rapidly changing direction due to noise in the stochastic, minibatch-based, estimate of the gradient. When the objective function remains constant for long periods of time, we do not know whether the parameters are stuck in a flat region, oscillating around a local minimum, or tracing their way around the perimeter of a large obstacle.

In this paper, we introduce a simple technique for qualitatively analyzing objective functions. We simply evaluate $J(\theta)$ at a series of points $\theta = (1 - \alpha)\theta_0 + \alpha\theta_1$ for varying values of α . This sweeps out a line in parameter space. We can see whether the cross-section of the objective function along this line is well-behaved.

When we set $\theta_0 = \theta_i$ and $\theta_1 = \theta_f$, we find that the objective function has a simple, approximately convex shape along this cross-section. In other words, if we knew the correct direction, a single coarse line search could do a good job of training a neural network.

These results are consistent with recent empirical and theoretical work arguing that local minima are not a significant problem for training large neural networks (Saxe et al., 2013; Dauphin et al., 2014; Choromanska et al., 2014).

3 FEED-FORWARD FULLY CONNECTED NETWORKS

We begin our investigation with the simplest kind of neural network, the deterministic, feed-forward, fully-connected supervised network. For these experiments we use the MNIST dataset (LeCun et al., 1998). When not using dataset augmentation, the best result in this category is a maxout network (Goodfellow et al., 2013c) regularized with dropout (Srivastava et al., 2014) and adversarial training (Goodfellow et al., 2014), and trained using SGD with momentum. See the appendix of this paper for a full specification of the architecture and training algorithm for this and all subsequent experiments. This configuration results in an average of 78.2 mistakes on the MNIST test set, out of 10,000 examples total. Without adversarial training, the model also performs very well, with only 94 mistakes. Running the linear interpolation experiment on this problem, we find in Fig. 1 that the 1-D subspace spanning the initial parameters and final parameters is very well-behaved, and that SGD spends most of its time exploring the flat region at the bottom of the valley. Maxout units do not saturate (they can saturate with respect to their input, but not with respect to their parameters), so perhaps it should not be too surprising that optimization is simple in this case. To determine whether the hard zero saturation of ReLUs (Jarrett et al., 2009; Glorot et al., 2011) or the two-sided saturation of logistic sigmoids can induce additional difficulties, we ran the linear interpolation experiment for both of these activation functions. The results are presented in Fig. 2 and Fig. 3. Again, we find that the 1-D subspace spanning the initial and final parameters contains no difficult, exotic structures.

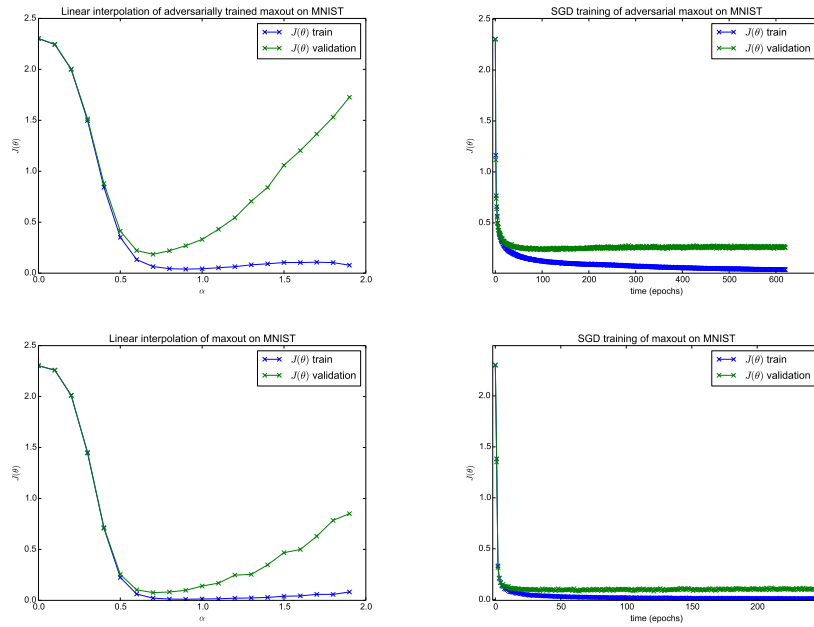


Figure 1: Experiments with maxout on MNIST. Top row) The state of the art model, with adversarial training. Bottom row) The previous best maxout network, without adversarial training. Left column) The linear interpolation experiment. This experiment shows that the objective function is fairly smooth within the 1-D subspace spanning the initial and final parameters of the model. Apart from the flattening near $\alpha = 0$, it appears nearly convex in this subspace. If we chose the initial direction correctly, we could solve the problem with a coarse line search. Right column) The progress of the actual SGD algorithm over time. The vast majority of learning happens in the first few epochs. Thereafter, the algorithm struggles to make progress.

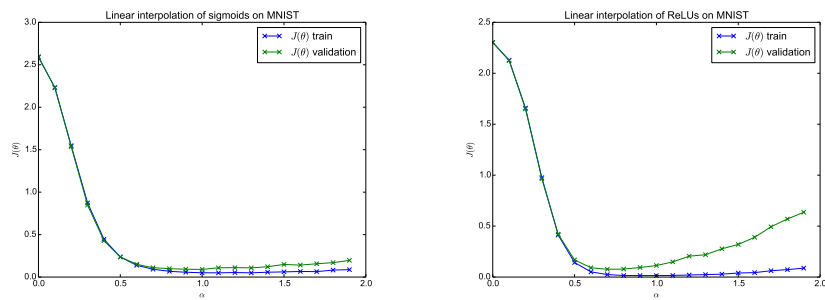


Figure 2: The linear interpolation curves for fully connected networks with different activation functions. Left) Sigmoid activation function. Right) ReLU activation function.

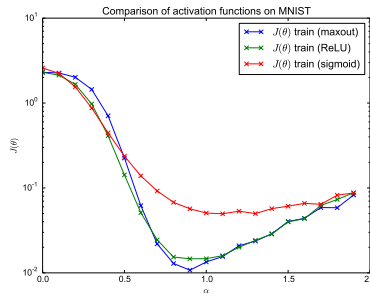


Figure 3: The linear interpolation experiment for maxout, ReLUs, and sigmoids on MNIST, all plotted on the same axis for comparison. For this plot, we put the y axis in log scale, otherwise differences at the bottom of the curve are difficult to see.

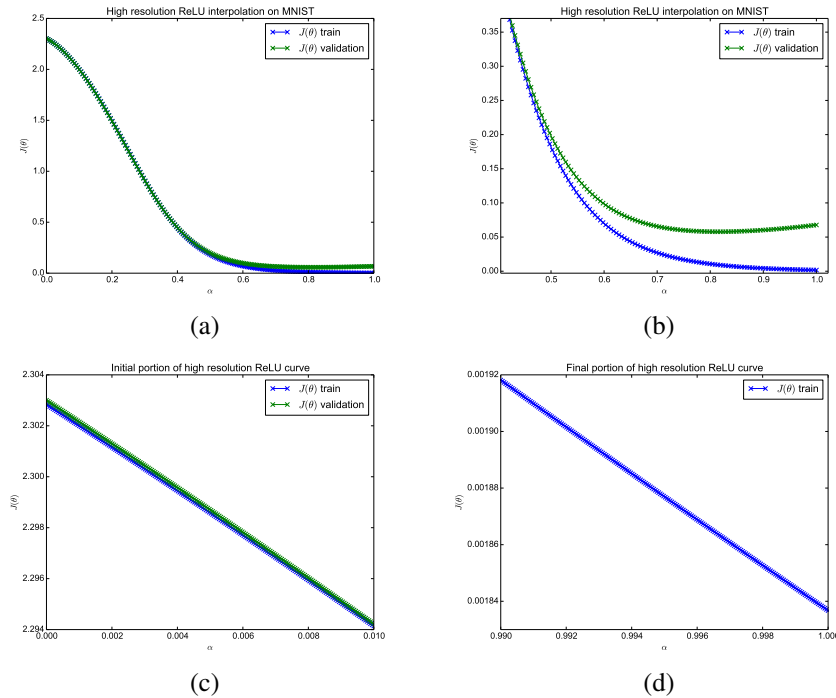


Figure 4: Higher resolution linear interpolation experiments. a) Tiling the interval $[0, 1]$ with 200 values of α . b) A zoomed-in view of the same plot. c) Tiling the interval $[0, .01]$ with 200 values of α , to see whether the initial symmetry breaking causes difficult structures. d) Tiling the interval $[\.99, 1.]$ with 200 values of α , to see if the behavior of the objective function is more exotic in regions where the parameters encode fully learned intermediate concepts. We do not show the validation set objective here because it is too widely separated from the training set objective and would require zooming out the plot too far.

One possible objection to these results is that we have explored α with too coarse of a resolution to expose local non-convex structures. We therefore ran a variety of higher-resolution experiments, presented in Fig. 4. For these experiments, we did not use dropout, because the resolution we use here is high enough to expose artifacts induced by the Monte Carlo approximation to the true dropout loss function, which involves a sum over all (exponentially many) dropout masks. Maxout tends to overfit on MNIST if used without dropout, so we used ReLUs for these experiments. We found that increased resolution did not expose any small, difficult structures.

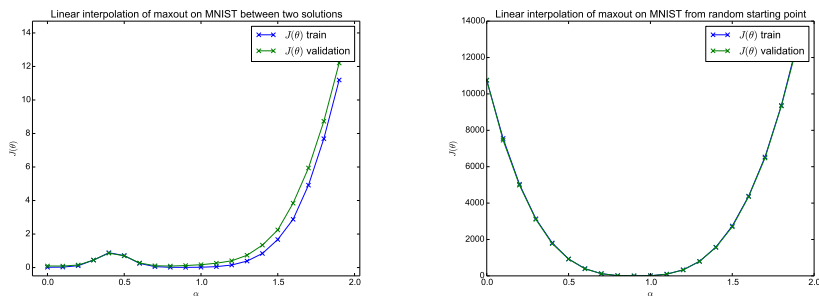


Figure 5: Here we use linear interpolation to search for local minima. Left) By interpolating between two different SGD solutions, we show that each solution is a different local minimum within this 1-D subspace. Right) If we interpolate between a random point in space and an SGD solution, we find no local minima besides the SGD solution, suggesting that local minima are rare.

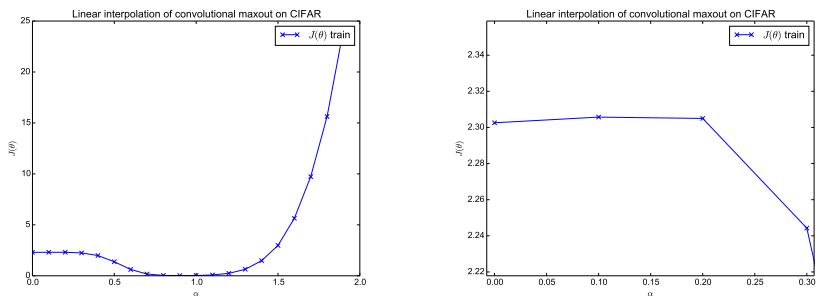


Figure 6: The linear interpolation experiment for a convolutional maxout network on the CIFAR-10 dataset (Krizhevsky & Hinton, 2009). Left) At a global scale, the curve looks very well-behaved. Right) Zoomed in near the initial point, we see there is a shallow barrier that SGD must navigate.

There are of course multiple minima in neural network optimization problems, and the shortest path between two minima can contain a barrier of higher cost. We can find two different solutions by using different random seeds for the random number generators used to initialize the weights, generate dropout masks, and select examples for SGD minibatches. (It is possible that these solutions are not minima but saddle points that SGD failed to escape) We do not find any local minima within this subspace other than solution points, and these different solutions appear to correspond to different choices of how to break the symmetry of the saddle point at the origin, rather than to fundamentally different solutions of varying quality. See Fig. 5.

4 ADVANCED NETWORKS

Having performed experiments to understand the behavior of neural network optimization on supervised feedforward networks, we now verify that the same behavior occurs for more advanced networks.

In the case of convolutional networks, we find that there is a single barrier in the objective function, near where the network is initialized. This may simply correspond to the network being initialized with too large of random weights. This barrier is reasonably wide but not very tall. See Fig. 6 for details.

To examine the behavior of SGD on generative models, we experimented with an MP-DBM (Goodfellow et al., 2013a). This model is useful for our purposes because it gets good performance as a generative model and as a classifier, and its objective function is easy to evaluate (no MCMC business). Here we find a secondary local minimum with high error, but a visualization of the SGD trajectory reveals that SGD passed far enough around the anomaly to avoid having it affect learning.

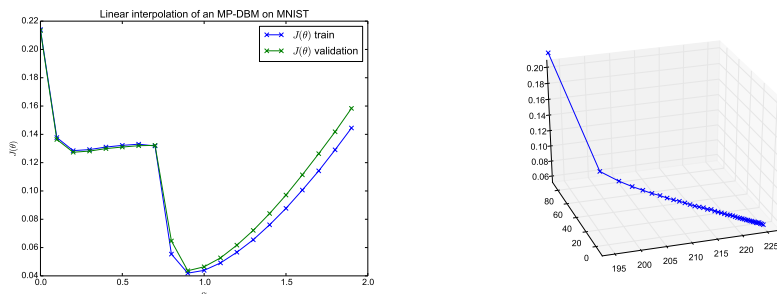


Figure 7: Experiments with the MP-DBM. Left) The linear interpolation experiment reveals a secondary local minimum with high error. Right) On the two horizontal axes, we plot components of θ that capture the extrema of θ throughout the learning process. On the vertical axis, we plot the objective function. Each point is another epoch of actual SGD learning. This plot allows us to see that SGD did not pass near this anomaly.

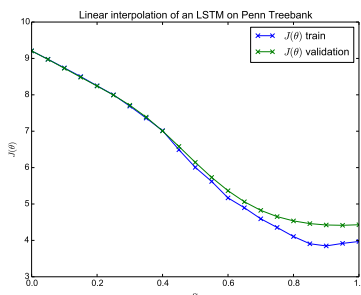


Figure 8: The linear interpolation experiment for an LSTM trained on the Penn Treebank dataset.

See Fig. 7. The MP-DBM was initialized with very large, sparse, weights, which may have contributed to our visualization technique exploring more non-convex areas, e.g. due to saturation of sigmoidal units.

Finally, we performed the linear interpolation experiment for an LSTM regularized with dropout (Hochreiter & Schmidhuber, 1997; Zaremba et al., 2014) on the Penn Treebank dataset (Marcus et al., 1993). See Fig. 8. This experiment did not find any difficult structures, showing that the exotic features of non-convex optimization do not appear to cause difficulty even for recurrent models of sequences.

5 DEEP LINEAR NETWORKS

Saxe et al. (2013) have advocated developing a mathematical theory of deep networks by studying simplified mathematical models of these networks. Deep networks are formed by composing an alternating series of learned affine transformations and fixed non-linearities. One simplified way to model these functions is to compose only a series of learned linear transformations. The composition of a series of linear transformations is itself a linear transformation, so this mathematical model lacks the expressive capacity of a general deep network. However, because the weights of such a model are factored, its learning dynamics resemble those of the deep network. The output of the model is linear in the input to the model, but non-linear as a function of the model parameters. In particular, while fitting linear regression parameters is a convex problem, fitting deep linear regression parameters is a non-convex problem.

Deep linear regression suffers from saddle points but does not suffer from local minima of varying quality. All minima are global minima, and are linked to each other in a continuous manifold.

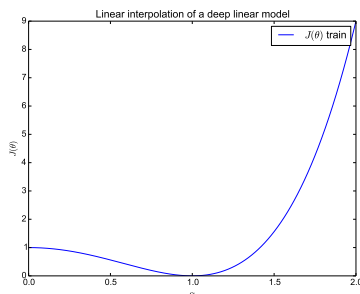


Figure 9: Linear interpolation from a small random initialization point to a solution for a linear regression model of depth 2. This shows the same qualitative features as our linear interpolation experiments for neural networks: a flattening of the objective function near the saddle point at the origin, and only one minimum within this 1-D subspace.

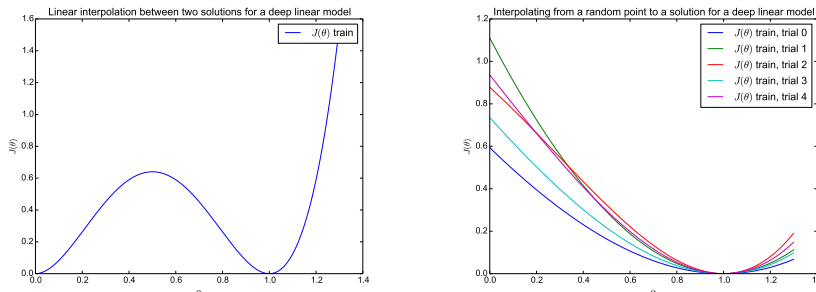


Figure 10: Left) Interpolation between two solutions to deep linear regression. Though these two solutions lie on connected manifold of globally minimal values, the straight line between them encounters a barrier of higher cost. The curve for the low dimensional linear model has all the same qualitative characteristics as the curve for the high dimensional non-linear networks we studied. Right) Interpolation between a random point with large norm and an solution to deep linear regression. As with the neural network, this search does not encounter any minima other than the solution used to initialize the search.

Our linear interpolation experiments can be carried out *analytically* rather than experimentally in the case of deep linear regression. The results are strikingly similar to our results with deep non-linear networks.

Specifically, we show that the problem of training $y = w_1 w_2 x$ to output 1 when $x = 1$ using mean squared error is sufficient to produce all of the qualitative features of neural network training that our linear interpolation experiments have exposed. See Fig. 9 and Fig. 10.

6 DISCUSSION

The reason for the success of SGD on a wide variety of tasks is now clear: these tasks are relatively easy to optimize. Finding a good direction in a high-dimensional space is a difficult problem, but it is not nearly as difficult as navigating an error surface that has complicated obstacles within multiple different low-dimensional subspaces.

This work has only considered neural networks that perform very well. It is possible that these neural networks perform well because extensive hyperparameter search has found problems that SGD is able to optimize easily, but that other hyperparameters correspond to optimization problems that are too hard. In particular, it seems likely that very large neural networks are easier to fit to a particular task.

Future work should aim to characterize the set of problems that are easy for SGD, to understand why SGD is able to avoid the obstacles that are present, and to determine why the training of large models remains slow despite the scarcity of obstacles. More advanced optimization algorithms could reduce the computational cost of deploying neural networks by enabling small networks to reach good performance, and could reduce the cost of training large networks by reducing the amount of time required to reach their solution.

ACKNOWLEDGMENTS

We would like to thank Jörg Bornschein, Eric Drexler, and Yann Dauphin for helpful discussions. We would like to thank Yaroslav Bulatov, Chung-Cheng Chiu, Greg Corrado, and Jeff Dean for their reviews of drafts of this work. We would like to thank the developers of Theano (Bergstra et al., 2010; Bastien et al., 2012) and Pylearn2 (Goodfellow et al., 2013b).

REFERENCES

- Bastien, Frédéric, Lamblin, Pascal, Pascanu, Razvan, Bergstra, James, Goodfellow, Ian J., Bergeron, Arnaud, Bouchard, Nicolas, and Bengio, Yoshua. Theano: new features and speed improvements. Deep Learning and Unsupervised Feature Learning NIPS 2012 Workshop, 2012.
- Bergstra, James, Breuleux, Olivier, Bastien, Frédéric, Lamblin, Pascal, Pascanu, Razvan, Desjardins, Guillaume, Turian, Joseph, Warde-Farley, David, and Bengio, Yoshua. Theano: a CPU and GPU math expression compiler. In *Proceedings of the Python for Scientific Computing Conference (SciPy)*, June 2010. Oral Presentation.
- Choromanska, A., Henaff, M., Mathieu, M., Ben Arous, G., and LeCun, Y. The Loss Surface of Multilayer Networks. *ArXiv e-prints*, November 2014.
- Dauphin, Yann N, Pascanu, Razvan, Gulcehre, Caglar, Cho, Kyunghyun, Ganguli, Surya, and Bengio, Yoshua. Identifying and attacking the saddle point problem in high-dimensional non-convex optimization. In Ghahramani, Z., Welling, M., Cortes, C., Lawrence, N.D., and Weinberger, K.Q. (eds.), *Advances in Neural Information Processing Systems 27*, pp. 2933–2941. Curran Associates, Inc., 2014.
- Glorot, Xavier, Bordes, Antoine, and Bengio, Yoshua. Deep sparse rectifier neural networks. In *JMLR W&CP: Proceedings of the Fourteenth International Conference on Artificial Intelligence and Statistics (AISTATS 2011)*, April 2011.
- Goodfellow, Ian, Shlens, Jonathon, and Szegedy, Christian. Explaining and harnessing adversarial examples. 2014. URL <http://arxiv.org/abs/1412.6572>.
- Goodfellow, Ian J., Mirza, Mehdi, Courville, Aaron, and Bengio, Yoshua. Multi-prediction deep Boltzmann machines. In *Neural Information Processing Systems*, December 2013a.
- Goodfellow, Ian J., Warde-Farley, David, Lamblin, Pascal, Dumoulin, Vincent, Mirza, Mehdi, Pascanu, Razvan, Bergstra, James, Bastien, Frédéric, and Bengio, Yoshua. Pylearn2: a machine learning research library. *arXiv preprint arXiv:1308.4214*, 2013b.
- Goodfellow, Ian J., Warde-Farley, David, Mirza, Mehdi, Courville, Aaron, and Bengio, Yoshua. Maxout networks. In Dasgupta, Sanjoy and McAllester, David (eds.), *International Conference on Machine Learning*, pp. 1319–1327, 2013c.
- Hochreiter, S. and Schmidhuber, J. Long short-term memory. *Neural Computation*, 9(8):1735–1780, 1997.
- Jarrett, Kevin, Kavukcuoglu, Koray, Ranzato, Marc’Aurelio, and LeCun, Yann. What is the best multi-stage architecture for object recognition? In *Proc. International Conference on Computer Vision (ICCV’09)*, pp. 2146–2153. IEEE, 2009.
- Krizhevsky, Alex and Hinton, Geoffrey. Learning multiple layers of features from tiny images. Technical report, University of Toronto, 2009.

- LeCun, Yann, Bottou, Leon, Bengio, Yoshua, and Haffner, Patrick. Gradient-based learning applied to document recognition. *Proceedings of the IEEE*, 86(11):2278–2324, November 1998.
- LeCun, Yann, Kavukcuoglu, Koray, and Farabet, Clément. Convolutional networks and applications in vision. In *Circuits and Systems (ISCAS), Proceedings of 2010 IEEE International Symposium on*, pp. 253–256. IEEE, 2010.
- Marcus, Mitchell P., Santorini, Beatrice, and Marcinkiewicz, Mary Ann. Building a large annotated corpus of english: The penn treebank. *COMPUTATIONAL LINGUISTICS*, 19(2):313–330, 1993.
- Rumelhart, D. E., Hinton, G. E., and Williams, R. J. Learning internal representations by error propagation. volume 1, chapter 8, pp. 318–362. MIT Press, Cambridge, 1986.
- Saxe, Andrew M., McClelland, James L., and Ganguli, Surya. Exact solutions to the nonlinear dynamics of learning in deep linear neural networks. In *ICLR*, 2013.
- Srivastava, Nitish. Improving Neural Networks with Dropout. Master’s thesis, University of Toronto, Toronto, Canada, January 2013.
- Srivastava, Nitish, Hinton, Geoffrey, Krizhevsky, Alex, Sutskever, Ilya, and Salakhutdinov, Ruslan. Dropout: A simple way to prevent neural networks from overfitting. *The Journal of Machine Learning Research*, 15(1):1929–1958, 2014.
- Zaremba, Wojciech, Sutskever, Ilya, and Vinyals, Oriol. Recurrent neural network regularization. *CoRR*, abs/1409.2329, 2014. URL <http://arxiv.org/abs/1409.2329>.

A EXPERIMENT DETAILS

All of our experiments except for the sigmoid network were using hyperparameters taken directly from the literature. We fully specify each of them here.

Adversarially trained maxout network: This model is the one used by Goodfellow et al. (2014). There is no public configuration for it, but the paper describes how to modify the previous best maxout network to obtain it.

Maxout network: This model was retrained using the publicly available implementation used by Goodfellow et al. (2013c). The code is available at:

https://github.com/lisa-lab/pylearn2/blob/master/pylearn2/scripts/papers/maxout/mnist_pi.yaml

ReLU network with dropout: This model is intended to nearly reproduce the the dropout ReLU network described by Srivastava (2013). It is a standard reference implementation provided by Pylearn2 (Goodfellow et al., 2013b) and the specific file is available here:

https://github.com/lisa-lab/pylearn2/blob/master/pylearn2/scripts/papers/dropout/mnist_valid.yaml

ReLU network without dropout: We simply removed the dropout from the preceding configuration file.

Sigmoid network: We simply replaced the ReLU non-linearities with sigmoids. This performs acceptably for a sigmoid network; it gets a test set error rate of 1.66%.

Convolutional network: We used the best convolutional network available in Pylearn2 for the CIFAR-10 dataset, specifically the one developed by Goodfellow et al. (2013c). In order to reduce the computational cost of computing the training set objective, we used the the variant without data augmentation. The configuration file is available here: https://github.com/lisa-lab/pylearn2/blob/master/pylearn2/scripts/papers/maxout/cifar10_no_aug_valid.yaml

MP-DBM: We used the best MP-DBM for classifying MNIST, as described by Goodfellow et al. (2013a).

Dropout LSTM: We used the configuration described in the paper introducing this method (Zaremba et al., 2014).

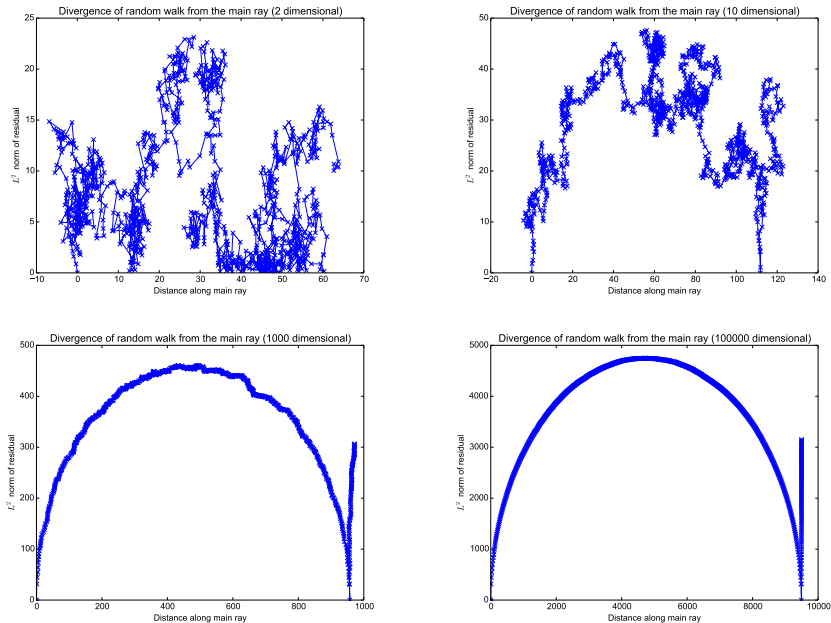


Figure 11: Plots of the projection along the axis from initialization to solution versus the norm of the residual of this projection for random walks of varying dimension. Each plot is formed by using 1,000 steps. We designate step 900 as being the “solution” and continue to plot 100 more steps, in order to simulate the way neural network training trajectories continue past the point that early stopping on a validation set criterion chooses as being the solution. Each step is made by incrementing the current coordinate by a sample from a Gaussian distribution with zero mean and unit covariance. Because the dimensionality of the space forces most trajectories to have this highly regular shape, this kind of plot is not a meaningful way of investigating how SGD behaves as it moves away from the 1-D subspace we study in this paper.

B STRAYING FROM THE PATH

We have shown that, for seven different models of practical interest, there exists a straight path from initialization to solution along which the objective function decreases smoothly and monotonically, at least up to the resolution that our experiments investigated.

Stochastic gradient descent does not actually follow this path. We know that SGD matches this path at the beginning and at the end.

One might naturally want to plot the norm of the residual of the parameter value after projecting the parameters at each point in time into the 1-D subspace we have identified. SGD begins at θ_i , the solution point chosen by early stopping is θ_f , and SGD visits $\theta(t)$ at time t . If we define \mathbf{u} to be a unit vector pointing in the direction $\theta_f - \theta_i$, then the primary subspace we have investigated so far is the line $\theta_i + \alpha(t)\mathbf{u}$ where $\alpha(t) = (\theta(t) - \theta_i)^\top \mathbf{u}$. We can plot the coordinate within this subspace, $\alpha(t)$, on the horizontal axis. We can then define a second unit vector \mathbf{v} pointed in the direction $\theta(t) - (\theta_i + \alpha(t)\mathbf{u})$. The projection into this subspace is $\beta(t) = (\theta(t) - \theta_i - \alpha(t)\mathbf{u})^\top \mathbf{v}$. In other words, $\beta(t)$ is the norm of the residual of the projection of θ_i onto the line spanning initialization and solution. We can plot β on the vertical axis.

In the next section, we will see that the shape of the objective function in terms of α and β coordinates has interesting features that vary from one problem to another. However, it is important to understand that this kind of plot does not tell us much about the shape of the SGD trajectory. All that it tells us is how far SGD strays from the primary linear subspace. This is because in high dimensional spaces, the shape of this curve does not convey very much information. See Fig. 11 for a demonstration of how this plot converges to a simple geometric shape as the dimensionality of a random walk increases.

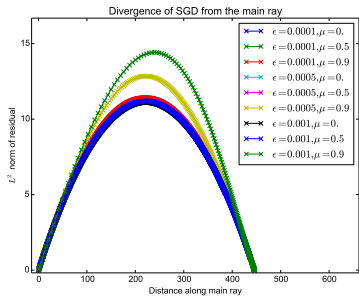


Figure 12: To show the effect of different learning rates ϵ and momentum coefficients μ , we plot the projection and residual norm of gradient descent with several different hyperparameters. In this case, to make the plots comparable, we use the true solution to a synthetic, convex problem as the endpoint for all trajectories. (In the non-convex case, different trajectories could go to different solutions, and this would confound our interpretation of the differences between them) Because this problem is 100,000 dimensional, the curves all have a very simple shape, and the primary quantity distinguishing them is the maximum norm of the residual.

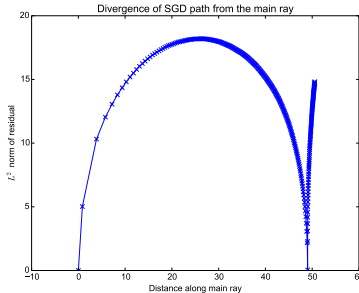


Figure 13: This plot examines how far off the linear path SGD strays when training a maxout network on MNIST. The x axis is the projection along the linear path from initialization to solution. The y axis is the norm of the residual. The plot uses the L^p norm with $p = 2$, also known as the Euclidean norm. It is not the squared norm.

Plots of the residual norm of the projection for SGD trajectories converge to a very similar geometric shape in high dimensional spaces. See Fig. 12 for an example of several different runs of SGD on the same problem. However, we can still glean some information from this kind of plot by looking at the maximum norm of the residual and comparing this to the maximum norm of the parameter vector as a whole.

We show this same kind of plot for a maxout network in Fig. 13. Keep in mind that the shape of the trajectory is not interesting, but the ratio of the norm of the residual to the total norm of the parameter vector at each point does give us some idea of how much information the 1-D projection discards. We see from this plot that our linear subspace captures at least $2/3$ the norm of the parameter vector at all points in time.

C THREE-DIMENSIONAL VISUALIZATIONS

A natural question is whether there exist obstacles in between the well-behaved linear subspace we have described and the path followed by SGD. One way to investigate this is to introduce an additional direction of exploration. Specifically, we would like to explore the line passing through each SGD point and its projection on the primary 1-D subspace we have investigated so far. If this line contains obstacles, it could explain why SGD does not exploit the simple behavior within this subspace.

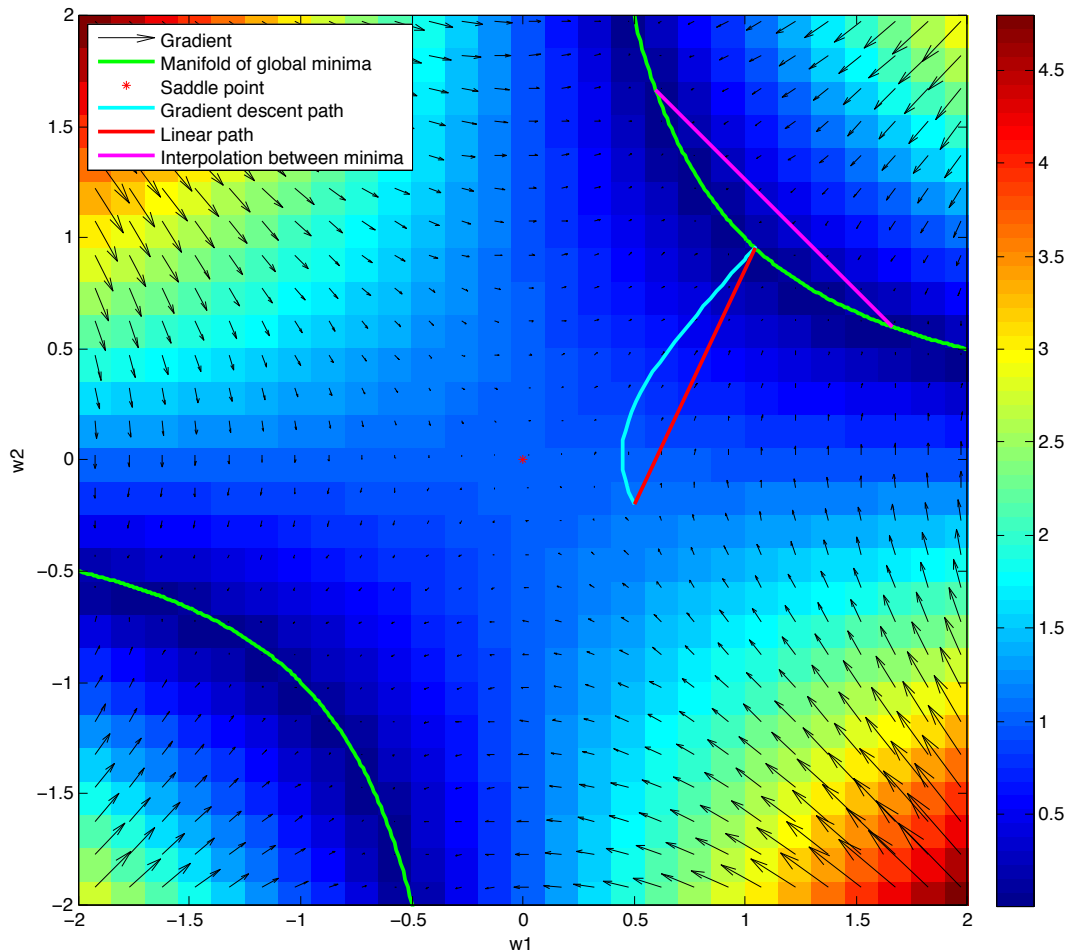


Figure 14: The error surface $(1 - w_1 w_2)^2$ of a factored linear model with two layers and one unit per layer. This error surface shows a saddle point at the origin and a non-linear manifold of global solutions. The SGD trajectory from initialization to solution encounters negative curvature near its initial point and positive curvature near its final point, but does not encounter any exotic obstacles.

For our factored linear model, where the training loss is just $(1 - w_1 w_2)^2$, we can accomplish this by viewing a heatmap of the cost function. See Fig 14. This figure predicts many properties that we expect to see for our more complicated neural network models: negative curvature at initialization, positive curvature surrounding the solution, a lack of obstacles separating the SGD trajectory from the well-behaved region of the function, and a connected manifold of globally optimal points. In this case, the connected manifold is the hyperbola $w_2 = 1/w_1$. For neural networks, the pattern of equivalent solutions will be different. For example, we can take a deep rectified linear network and obtain an equivalent network by rescaling its parameters. If we modify the parameters of layer i by multiplying bias j and column j of the weight matrix by γ , then we can preserve the function of the input that the network represents by dividing row j of the weights for layer $i + 1$ by γ . In the case of the factored linear model, the hyperbolic shape of this manifold means that linearly interpolating between two solution points reveals a region of high cost in the middle, even though the two solutions are connected by a manifold of other solutions.

This kind of 3-D plot is not directly achievable for problems with more than two parameters. We must summarize the parameters with a 2-D coordinate somehow. In the remainder of this section, we summarize the parameters via their projection in to the line spanning initialization and solution (the $\alpha(t)$ coordinate defined in the previous section) and their projection into the line orthogonal to this subspace that passes through the SGD point $\theta(t)$, which we defined as the coordinate $\beta(t)$ in the previous section.

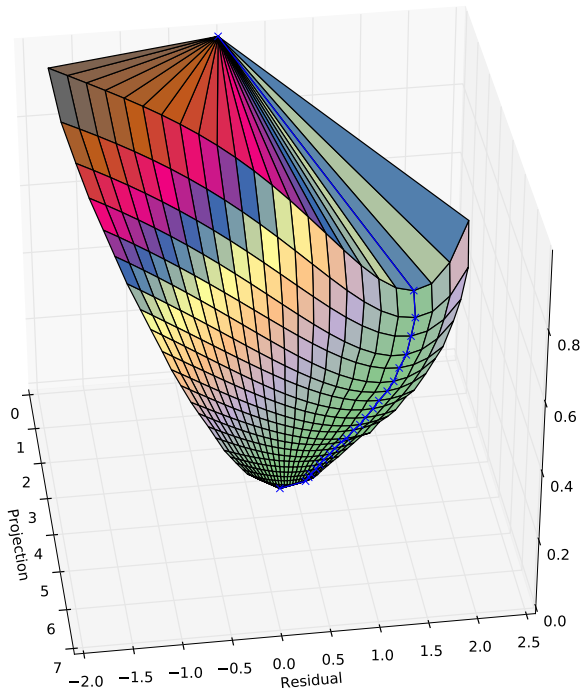


Figure 15: As a canonical example of the deep factored linear model of deep network training, we trained a linear model with mean squared error on MNIST. Specifically, we multiply together ten matrices, the first nine of which are square and have the same dimension as the MNIST input, and the last of which has only ten columns. The output is thus a ten dimensional vector. The mean squared error encourages element i of this vector to have value close to 1 and the other elements to have zero when the true class is i . This 3-D plot shows negative curvature near the initialization point, positive curvature near the solution point, and a general lack of obstacles.

If we plot the cost as a function of α and β , we see that the cost function of a deep factored linear model (Fig. 15) has roughly the same structure as the cost function of our LSTM (Fig. 16) and as most of our feedforward networks (we show one in Fig. 17). These models show only structures predicted by the factored linear model of learning dynamics. However, for the adversarially trained maxout network, we find that an obstacle that is small in height yet very steep constrains SGD into a narrow canyon, preventing it from accessing the subspace studied in the main text of this paper (Fig. 18 and Fig. 19). Finally, recall that the MP-DBM had a local minimum within the primary 1-D subspace (which could be a local minimum or a saddle point in high dimensional space). With our 3-D plot (Fig. 20), we see that SGD passed far around the plateau surrounding this point.

Note that in most of these visualizations we can see significant negative curvature in the early part of the SGD trajectory, and that SGD does not seem to have any difficulty escaping the saddle point near the origin. One possible explanation for this behavior is that one model of SGD with sufficiently small step size naturally avoids saddle points. Consider the SGD trajectory as a function of time, $\theta(t)$. As an analytical model of SGD with small step size, we can consider the continuous-time gradient descent process with $\frac{d}{dt}\theta = -\nabla_{\theta}J(\theta)$. If we make a second-order Taylor series expansion

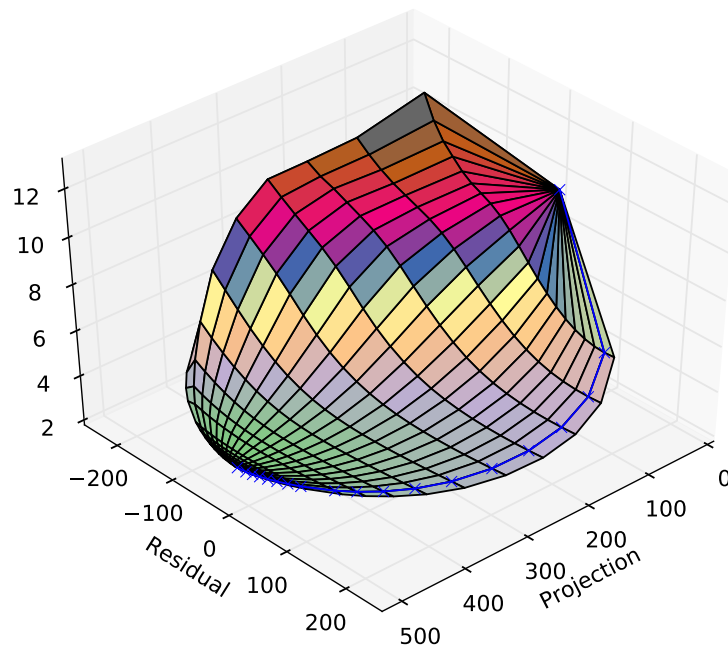


Figure 16: The 3-D visualization of the LSTM cost reveals a simple structure, qualitatively the same as that of the deep factored linear model.

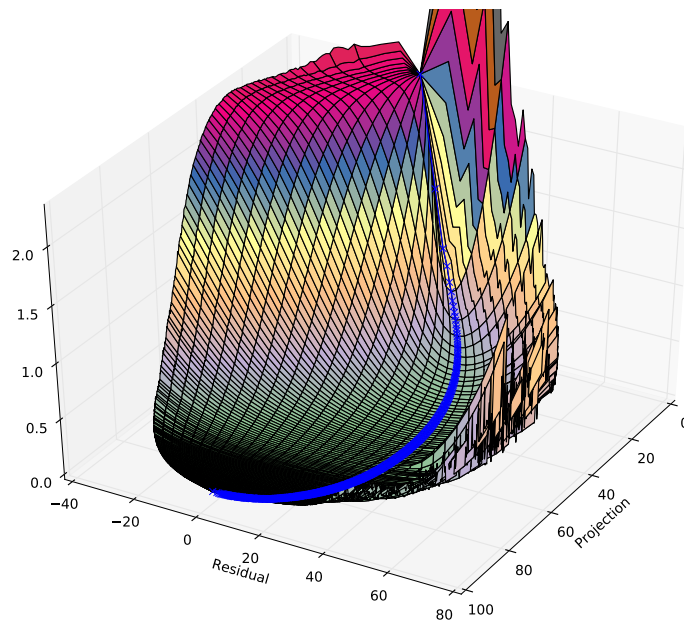


Figure 17: Most of our 3-D visualizations feedforward networks had shapes that were qualitatively the same as the factored linear network. Here we show the adversarially trained ReLU network as a representative sample.

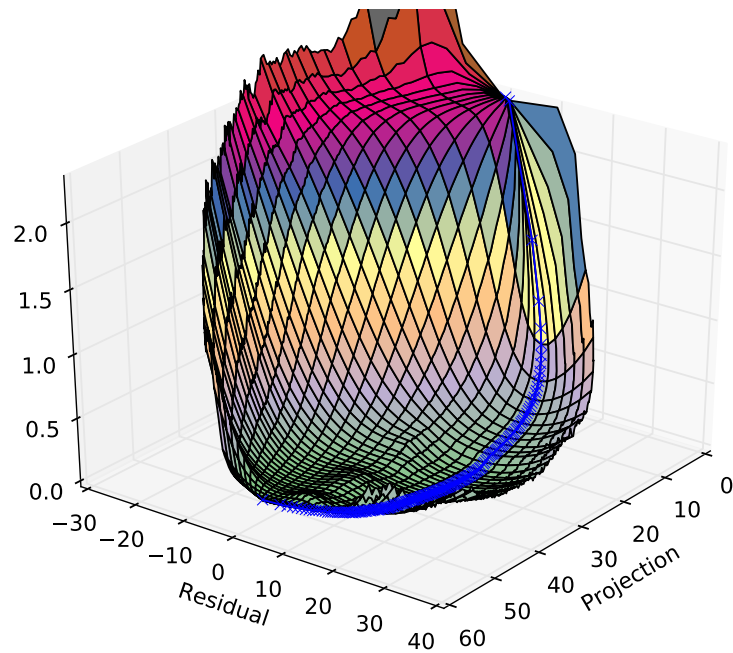


Figure 18: The 3-D visualization technique applied to adversarially trained maxout reveals some obstacles.

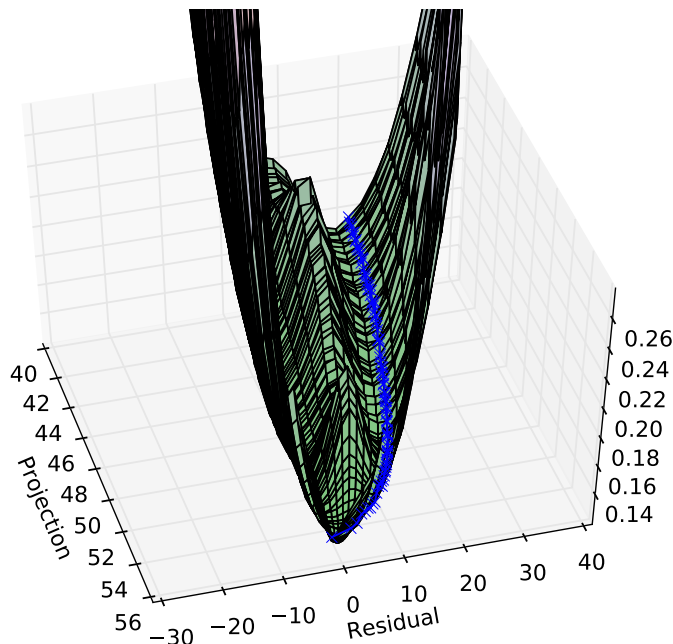


Figure 19: The same as Fig. 18, but zoomed in to show detail near the end of learning.

in time

$$\boldsymbol{\theta}(t) \approx \boldsymbol{\theta}(0) - t \frac{d}{dt} \boldsymbol{\theta}(t) + \frac{1}{2} t^2 \frac{d^2}{dt^2} \boldsymbol{\theta}(t)$$

it simplifies to

$$\boldsymbol{\theta}(t) \approx \boldsymbol{\theta}(0) - t \nabla_{\boldsymbol{\theta}(0)} J(\boldsymbol{\theta}(0)) + \frac{1}{2} t^2 \mathbf{H}(0) \nabla_{\boldsymbol{\theta}(0)} J(\boldsymbol{\theta}(0))$$

where \mathbf{H} is the Hessian matrix of $J(\boldsymbol{\theta}(0))$ with respect to $\boldsymbol{\theta}(0)$. This view shows that a *second-order approximation in time* of continuous-time gradient descent incorporates *second-order information in space* via the Hessian matrix. Specifically, the second-order term of the Taylor series expansion is equivalent to *ascending* the gradient of $\|\nabla_{\boldsymbol{\theta}} J(\boldsymbol{\theta})\|^2$. In other words, the first-order term says to go downhill, while the second-order term says to make the gradient get bigger. The latter term encourages SGD to exploit directions of negative curvature.

D CONTROL VISUALIZATIONS

Visualization has not typically been used as a tool for understanding the structure of neural network objective functions. This is mostly because neural network objective functions are very high-dimensional and visualizations are by necessity fairly low dimensional. In this section, we include a few “control” visualizations as a reminder of the need to interpret any low-dimensional visualization carefully.

Most of our visualizations showed rich structure in the cost function and a relatively simple shape in the SGD trajectory. It’s important to remember that our 3-D visualizations are not showing a 2-D linear subspace. Instead, they are showing multiply 1-D subspaces rotated to be parallel to each other. Our particular choice of subspaces was intended to capture a lot of variation in the cost function, and as a side effect it discards all variation in a high-dimensional trajectory, reducing most trajectories to semi-circles. If as a control we instead plot a randomly selected 2-D linear subspace

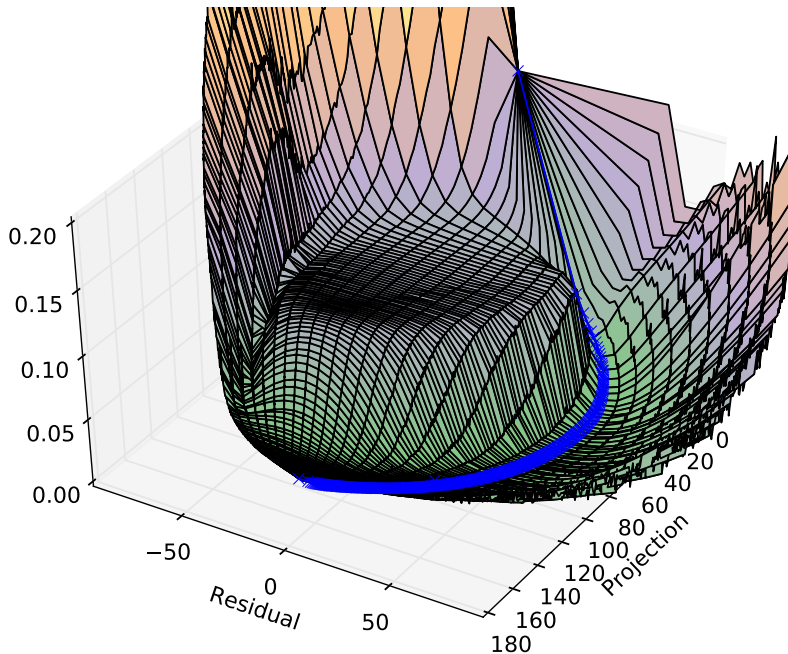


Figure 20: The 3-D visualization of the MP-DBM contains a plateau, but SGD avoided it.

intersecting the solution point, then we see that there is almost no variation in the cost function within this subspace, and the SGD trajectory is quite noisy. See Fig. 21.

As an intermediate control, we generated the plot for the MP-DBM, with $\alpha(t)$ on one axis, and the other axis being a random linear projection. This allows us to see a true 2-D linear subspace that has significant variation in the cost function due to the choice of the first axis, but also allows us to see that the SGD trajectory is not a semi-circle. See Fig. 22

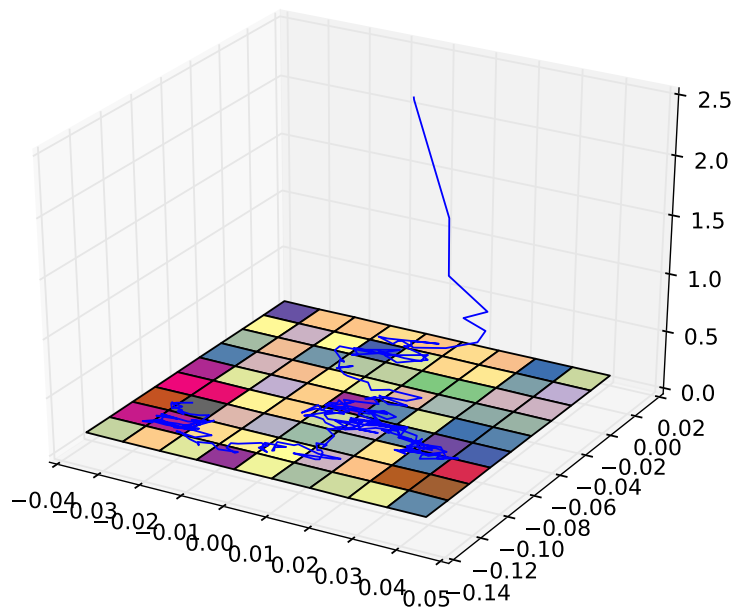


Figure 21: As a control experiment, we plot a random 2-D subspace intersecting the solution point. In this subspace, we see a complicated SGD trajectory and essentially no variation in the cost function value. This visualization is useful as a reminder that the visualizations presented in this paper are designed to expose variation in the cost function and discard variation in the shape of SGD trajectory. Not all directions in the cost function have high variability and SGD trajectories do vary greatly.

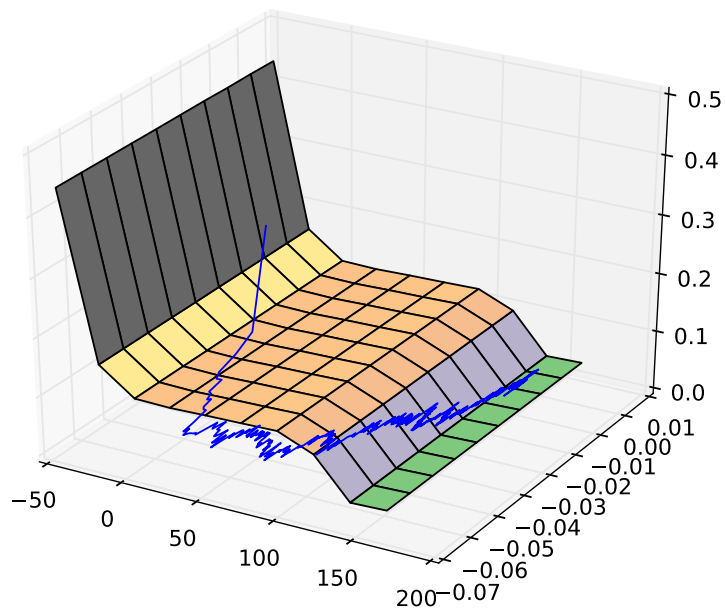


Figure 22: A control experiment with $\alpha(t)$ on one axis and the other axis being a random projection.